African Journal of Pure & Applied Sciences

ISSN: 2710-0758
DOI 10.33886/ajpas.v3i1.260

Journal homepage: http://journal.ku.ac.ke/index.php/AJPAS

Research Article Open Access

Effects of zinc oxide nanostructures on performance of natural dye sensitized solar cells

Njiru J. L. N.[1*], Migwi C. M.[1], Mwangi I. W.[1], Ngari R. W.[1]

[1*,1]Department of Physics, Kenyatta University, P.O. Box, 43844–0100, Nairobi, Kenya.

[1*]Corresponding Author's Email: njiru.lincon@students.ku.ac.ke

Received: 28th September 2021 / Accepted: 1st March 2022 / Published online: 1st June 2022

How to Cite:

Njiru, J., Migwi, C., Mwangi, I., & Ngari, R. (2022). Effects of zinc oxide nanostructures on performance of natural dye sensitized solar cells. *African Journal of Pure and Applied Sciences*, *3*(1), 185-201. https://doi.org/10.33886/ajpas.v3i1.260

ABSTRACT

Dye Sensitized Solar Cell (DSSC) is a very promising development in photovoltaic technology. In DSSCs, dye molecules provide the charges, while a semiconductor collects and transports the charge. The performance of DSSCs depend on the choice of nanostructure, semiconductor material and dye type. In this research we investigate the effect of ZnO nanostructures on the performance of DSSCs when sensitized with different natural dyes. We prepared ZnO nanoparticles (NPs), Long ZnO nanowires (NWs) and Long Branched ZnO NW films on Fluorine-doped Tin Oxide Transparent Conducting Oxide (FTO-TCO) glass, and determined their surface morphologies. Analysis software showed that ZnO NPs with a mean diameter of 36.39 nm had been deposited, Long ZnO NWs a with mean diameter of 60.59 nm and length of 22.03 µm had been grown and ZnO NW branches with a mean diameter of 36.88 nm and a length of 3.475 µm had grown on the parent NWs. Absorbance spectrum of anthocyanin dye extracted from mulberries, chlorophyll dye from spinach leaves and a dye blend in the ratio 1:1 were obtained and analyzed. The blended dye had better absorption features than the individual dyes; it had three absorption peaks one (highest) in the UV zone (363 nm) and two in the visible zone (523 nm and 676 nm) compared to two peaks each for anthocyanin and chlorophyll. It also had the widest full width at half maximum of 117.46 nm compared to 70.20 nm and 74.99 nm for anthocyanin and chlorophyll respectively. We assembled DSSCs using a platinum counter electrode and lithium iodide electrolyte and did I-V characterization. I-V results showed that DSSCs assembled with Long Branched ZnO NW photoanode and sensitized with any of the three dyes always performed better. The blended dye, when used to sensitize any of the three photoanodes, performed better than pure dyes. The best solar cell parameters were obtained when Long Branched ZnO NW DSSC was sensitized with cocktail dye giving open circuit voltage, $V_{oc} = 359$ mV, short circuit current, $I_{sc} = 2.16$ mA and efficiency, $\eta = 0.726\%$. The least performing DSSC was from ZnO NPs sensitized with chlorophyll dye with open circuit voltage, $V_{oc} = 320$ mV, short circuit current, $I_{sc} = 1.28$ mA and efficiency, $\eta = 0.303\%$.

Keywords: Dye sensitized solar cell, ZnO, Photoanode, Nanostructures, Organic dye, Solar cell parameters.

INTRODUCTION

Worldwide demand for energy is expected to double by the year 2050 and triple by the end of 21st century (Hess, 2005). Abundant supply of clean energy is a major global concern because most of energy comes from fossil fuels whose burning causes global warming and other environmental problems. Solar energy is cheap, abundant and clean and, if effectively harnessed, can provide an outright solution to global energy needs. Solar energy is used for electricity generation, photochemical processes, solar propulsion, solar desalination and room temperature control (Chu and Meisen, 2011). The aim of many researchers is to collect and convert solar energy to electrical energy because this form of energy has wide applications with deep impact on society.

Solar energy converted to electricity presents the greatest hope of meeting worldwide demand for clean and low-cost energy. This has led to the development of many photovoltaic technologies. Silicon-based solar cells

dominate the market today, but they are unable to meet the global demand of US $0.40 kW h^{-1} for low-cost energy (Zhang *et al.*, 2009). Silicon-based solar cells have undergone several developments, the first of which was wafer-based silicon cells which were made of crystalline silicon with materials such as monocrystalline, polycrystalline, amorphous silicon and hybrid silicon (Green, 2003). The second was thin-film silicon solar cells where a layer of micrometers thick semiconductor material is used. Thin-film solar cells are classified as amorphous silicon solar cells and non-silicon solar cells such as cadmium telluride and copper indium gallium (di) selenide (Md Yunus *et al.*, 2015). Dye Sensitized Solar Cell (DSSC) is an innovative thin-film technology employed to change the concept of two distinctive p and n layers used in p-n junction devices by using an electrochemical mechanism. Though their efficiencies have been relatively low compared with silicon-based solar cells, they use simple construction methods and they are made of low cost materials (Chopra *et al.*, Dutta, 2004). DSSC is made of a photo electrode and a counter electrode in a sandwich arrangement shown in Figure 1.

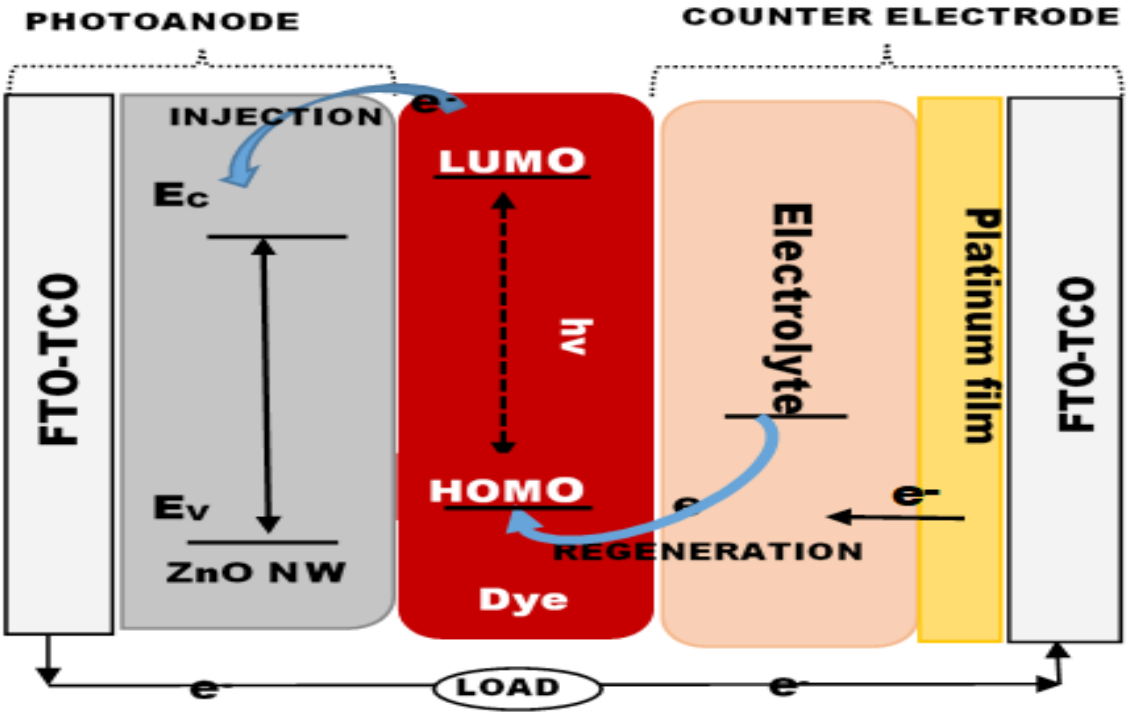

Figure 1: Schematic representation of components of DSSC

The photoanode is made of a wide band gap nanostructured semiconductor material deposited on a transparent conducting oxide glass substrate. The counter electrode is made of a good catalytic material deposited on a Transparent Conducting Oxide (TCO) glass substrate and a liquid electrolyte. The other very important component of a DSSC is dye sensitizer which forms the start of photovoltaic activity. When sunlight falls on a dye molecule it excites it to a higher energy level, leading to the formation of an exciton. Separation of electrons and holes is done through kinetic competition as in photosynthesis (Martín *et al.*, 2016). Electrons are then transferred to the conduction band of a wide band gap semiconductor for transport, while the holes are left in the dye material. The electrons will then be recovered by the electrolyte after they flow through the load. The efficiency of DSSCs depends on how effectively electrons are transported through the conduction band and recovered in the electrolyte. Since their discovery by O'Regan and Grätzel (1991), most work on DSSCs has used TiO_2 as the semiconductor recording the highest conversion efficiency of 11.3% (Chen *et al.*, 2009). Less work has been done on other potential semiconductors like ZnO which, apart from also being abundant and of low cost, has other unique properties, such as higher electronic mobility favorable for electron transport, reduced recombination losses (Yeo and Ko, 2014), and ease of crystallization and anisotropic growth, which allows it to be produced in various nanostructures. These nanostructures, when used for the photoanode in DSSCs, have various effects: they affect the way dye is adsorbed, they determine the way incident light is manipulated and managed, and they affect the way carriers are collected and transported. When semiconductor nanostructures are in nanoscale, the surface area is significantly increased compared to that of the corresponding bulk material (Onyia *et al.*, 2020). Nanoscale also increases the speed of electron transport by reducing the electron mean free path, and brings in

quantum confinement effects which increase the efficiency of electron collection by restricting electrons to specific energy levels (Zhang and Cao, 2011). Furthermore, semiconductor materials in nano-form can be synthesized into various nano-morphologies with various size and shapes, thus modifying the properties of the DSSCs. An essential factor in modifying the nanostructures of semiconductors is to prevent the electrons and holes from recombining upon excitation. Various deposition methods are used to achieve different morphologies with the idea of modifying the physical properties of the photoanode. ZnO nanowire (NW) structure has unique features for application in DSSCs: NWs have high aspect ratios, quantum confinement and direct paths for electrons, which lead to high electron diffusion coefficients (Xia *et al.*, 2003). In additional, adsorption of dye to NWs is known to be better than in tortuous pores of nanoparticle (NP) film (Cheng *et al.*, 2008).

The essential role of a dye in DSSCs is to convert solar energy into electricity. Materials used for the dye in DSSCs should have a small band gap energy to absorb photons of low energies. The dye should also be stable for over 180 times the redox reaction time to prolong cell lifetime (Hara and Mori, 2011). In most cases, inorganic dye materials comprising of metal complexes of ruthenium, osmium, metal porphyrin, phthalocyanine and inorganic quantum dots are used as dye materials (Adedokun *et al.*, 2016). However, in the recent past organic dye materials have become a worthwhile substitute to the expensive inorganic sensitizers. For instance, Kabir *et al.* (2019) assembled cells with efficiencies of 0.466% and 0.531% by sensitizing TiO_2 nanostructures with green spinach and red spinach dyes, respectively. Ossai *et al.* (2020) fabricated a cell with an efficiency of 0.75% by sensitizing ZnO NP cells with beetroot dye. Therefore, to further lower the cost of DSSCs we choose to use organic dyes as a substitute to expensive inorganic metal complex dyes. Organic dyes have been found to also have low energy payback time, perform better in low lighting and to have a variety of structures for various designs (Chen *et al.*, Huang, 2007). The absorption characteristics of a dye is a major contributor to the efficiency of DSSCs. The dye should have large light harvesting capacity in UV, VIS and NIR up to above 930 nm. The energy of the excited state should be above the electronic ground state corresponding to the ideal band gap of a single band gap solar cell (Green, 1982). The quality of a dye is determined by the ability of the dye to absorb light and inject electrons into the conduction band of the semiconductor before the electrons can have time to be recaptured by the oxidized sensitizer. This paper aims to compare the performance of DSSCs when different ZnO nanostructure photoanodes are sensitized with pure and blended organic dyes.

METHODOLOGY

The following materials were purchased to carry out the experiments in this work: fluorine-doped tin oxide (FTO)-TCO glass substrates (F: SnO_2-doped), zinc acetate dehydrate ($Zn(CH_300)_2.2H_2O$) 99.5% pure and Mw of 219.50 g mol^{-1}, methanol AR 99.8% pure, acetone 99.9% pure and Mw of 58.08 g mol^{-1}, ethanol 99.9% pure and Mw of 46.07 g mol^{-1}, anhydrous sodium hydroxide ($NaOH$) 98.0% pure, zinc nitrate hexahydrate ($Zn(NO_3)_2.6H_2O$) 98.0% pure and 297.4g Mw, hexamethylenetetramine (HMTA) ($C_6H_{12}N_4$) 99.0% pure and Mw 140.19 g mol^{-1}, polyethyleneimine (PEI) Mw ~ 800 g by Ls and average Mn ~ 600, ammonium hydroxide (NH_4OH) Mw 17.03 g mol^{-1} with 25.0% NH_3, lithium iodide from, platinum paste (platisol T/SP), thermoplastic sealing film (60 µm thick with 60 µm protection foil), scotch magic tape #810 (50 µm thick), five 50 ml syringes with needles, surgical blades and hot pressing tool. Mulberry fruits and spinach leaves were used for extraction of dyes.

Sample preparation

The working electrode and the counter electrode were prepared by depositing ZnO thin films on FTO-TCO glass substrates. The deposition of thin films and extraction of dyes was done at Kenyatta University and analysis of the samples was done in the Physical and Biological Sciences laboratories at Chuka University, University of Nairobi and University of Pretoria.

Preparation of Long Branched ZnO NWs

This was done in three stages: seeding of FTO-TCO with ZnO NPs, growth of Long ZnO and branching of Long ZnO as shown in Figure 2. In each stage we left behind a set of samples for analysis and characterization.

Deposition of ZnO NPs

The purchased FTO-TCO glasses were first cut into smaller pieces measuring $15\ mm \times 15\ mm \times 3\ mm$. The glass substrates were handled with care to prevent scratches on the conducting side. Before any deposition was done, the glass slides were cleaned with de-ionized water, followed by a mixture of ethanol and acetone in a sonic cleaner for 10 min, and then air dried. A margin of 5 mm was covered on two parallel sides of the conductive side of the glasses using scotch magic™ (Matte finish). The seeding solution was prepared by dissolving zinc acetate in methanol to make 0.01 M solution. A quantity of 125 ml of this solution was then put in a burette and added dropwise to a well stirred 65 ml of 0.03 M sodium hydroxide in methanol. The mixture was then incubated in an oven maintained at $60°\ C$ for 2 h to complete the chemical reactions. The solution was then centrifuged at 2000 revolutions per min

for 10 min to separate the ZnO NPs. The supernatant was discarded, and fresh methanol infused to suspend the NPs (Xu and Sun, 2011). A thin film of ZnO NP seeds was then dispersed on the conductive side of 18 pieces of FTO-TCO glasses by the drop coating method using a micropipette. The solvent was allowed to evaporate for 30 min and the scotch magic tape removed. Annealing was done at 210^0 C for 30 min on a programmable hot plate to allow dense and uniform dispersion of the NPs. Six of the seeded ZnO NPs were stored, while the other 12 were used for the growth of NWs in the next step.

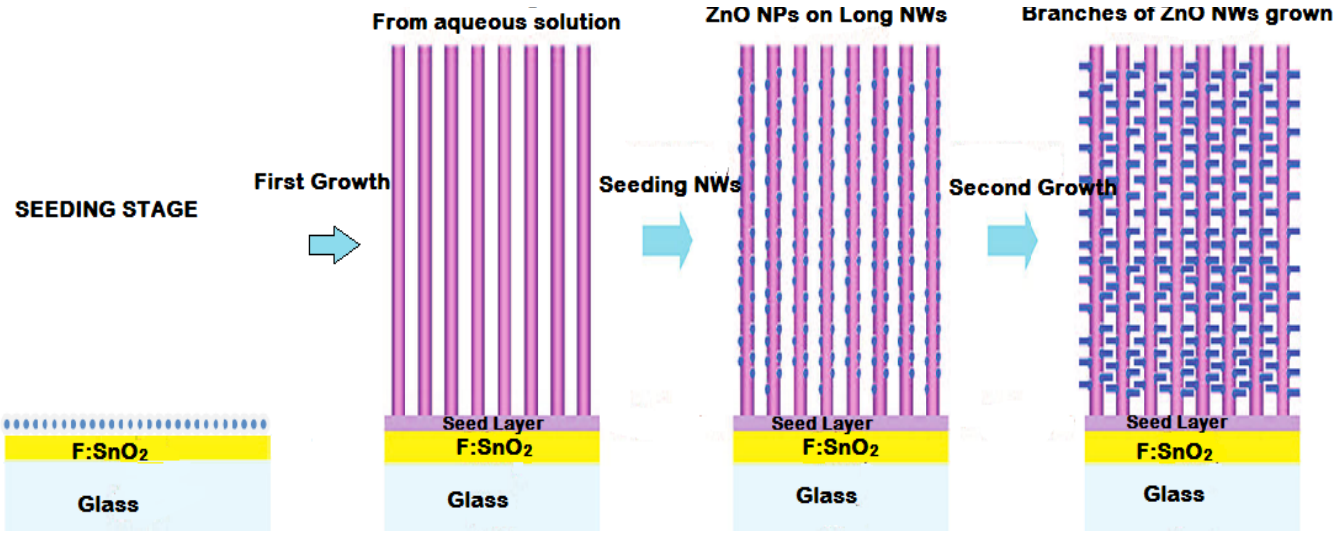

Figure 2: Schematic representation of steps for growth of ZnO NWs (Cheng et al., 2008)

Growth of long zinc Oxide nanowires

The NWs growth solution was prepared with 0.05 M zinc nitrate hexahydrate, 0.025 M HMTA, 0.005 M PEI, and 0.4 M ammonium hydroxide. Twelve beakers were filled with 40 ml of the preheated precursor solution, then the seeded glass substrates with margins of 5 mm covered with scotch magic tape and held firmly with non-reactive platinum wire suspended halfway in the solution with the seeded side facing down. The beakers were then sealed using aluminum foil and immediately placed in a programmable water bathe maintained at 88° C. The seeded substrates were left at this temperature for 12 h with replenishing being done after every 4 h for the NWs to grow. The pH of the precursor solution was measured using a pH meter at the 0 h, at 4 h (first replenishing), at 8 h (second replenishing) and at 12 h (at the end). After 12 h of growth the NWs were rinsed thoroughly using de-ionized water, the scotch magic tape removed, and then annealed at 450° C on the programmable hot plate for 35 min to remove any residue organics of HMTA and PEI polymers. (Cheng *et al.*, 2008; Xu *et al.*, 2009; Cheng and Fan, 2012). Six of the annealed ZnO NWs glasses were stored while the remaining six were used in the next step.

Branching of long zinc oxide nanowires

The six samples grown with NWs were seeded again by the drop-coating method and annealed at 210 °C. A branching precursor solution with approximately half the concentration of the solution used for the growth of Long ZnO NWs was prepared. The seeded Long ZnO NWs glasses were suspended in 40 ml of the branching precursor solution, sealed tightly with aluminum foil and placed in a water bath maintained at 88° C for 6 h to allow growth of NW branches. Replenishing was done after 3 h and the pH of the changed solution measured. The samples were carefully and thoroughly rinsed with de-ionized water, and then annealed in air at 450° C for 35 min. The Long Branched ZnO NWs samples were then stored in a sample holder for further analysis.

Deposition of counter electrode with platinum paste

Thoroughly cleaned and dried FTO-TCO glass substrates were held firmly on a bench using scotch magic™ (Matte finish) leaving a margin of 5 mm on all the sides. Doctor blade method was then used to deposit a thin film of platinum paste (Screen printable) by spreading a homogenous platinum layer using a glass rod (Berni *et al.*, 2004). The platinum thin films were annealed at 350° C for 20 min and stored in a blackened and sealed sample holder to keep them away from air and light.

Scanning Electron Microscopy (SEM) analysis of ZnO thin films

This was done using Atomic Force Microscopy (Zeiss Ultra PLUS FEG SEM[1]) at the University of Pretoria, South Africa. Samples were scanned with an electron beam to produce magnified images at high magnification and

resolution. Before SEM analysis samples were coated with ultrathin gold conductive surface. Important measurements were taken from the obtained SEM micrographs using ImageJ[2] software and the results analyzed using Origin[3] software.

Resistivity of thin films

The sheet resistivity of the solid samples was measured using the four probe method in which a computer was interfaced with a Keithely 2400 Source Meter Unit[4] (SMU) using LabVIEW. A Stylus Dektak Profilometer was used to estimate the resistivity of the deposited films. The diamond stylus was placed at the margin of the 5 mm left un-deposited with film for transmission of the Dektak sound through the film.

Preparation of natural dyes

To prepare pure undiluted anthocyanin and chlorophyll dye, 500 g of clean and fresh mulberry fruits and 500 g of clean, fresh and dry spinach leaves were first crushed in a mortar and incubated in 500 ml of acetone for 48 h at room temperature to ensure maximum extraction of the dye pigments. The mulberry fruit mixture and the chlorophyll mixture were separately filtered with an ordinary laboratory filter then with a filter paper with pores of approximately 0.1 µm to remove the solid dregs and impurities. A rotary vacuum evaporator was used to remove the solvent. Quantitation of dye concentrates was done by the dilution method using de-ionized water and an UV-1800 probe to obtain anthocyanin dye and chlorophyll dye of ≈ 0.5 M concentration. To make a cocktail dye, 20 ml of the diluted anthocyanin dye was mixed with 20 ml of diluted chlorophyll dye and thoroughly shaken for complete mixing.

Optical characterization of dye samples

The absorbance and reflectance data for the diluted anthocyanin dye, the chlorophyll dye and the cocktail dye blend were obtained using a Shimadzu UV-1800 UV/Visible Scanning Spectrophotometer. It was used to cover a wavelength range from 200-1100 nm. The absorbance results obtained were further analyzed using SpectraGryph 1.2.11 software to determine the concentration of the diluted dyes and to investigate optical parameters of the dyes.

Optical characterization ZnO films

Optical characterization of the FTO-TCO glass substrate, ZnO NP seeded glass, Long ZnO grown NW glass, Long Branched ZnO NW grown glass and Pt paste deposited counter electrode were done using the UV-1800 probe spectrophotometer. Raw transmittance and absorbance data were further analyzed using SpectraGryphy 1.2.11.

Assembling of DSSCs

DSSCs were assembled following the procedure described by Martineau (2012). ZnO photoanodes and platinum paste counter electrodes were put together with the active sides facing each other with 60 µm thick thermoplastic sealing film between them and then pressed with a hot-melt gasket. Good sealing of the DSSC was confirmed by visual examination to ensure the refractive indices of the gasket and glass substrate match. After sealing, the gap between the two electrodes was filled with lithium iodide electrolyte solution using a syringe. Figure 3 shows a layout of a fabricated Long Branched ZnO NW DSSCs.

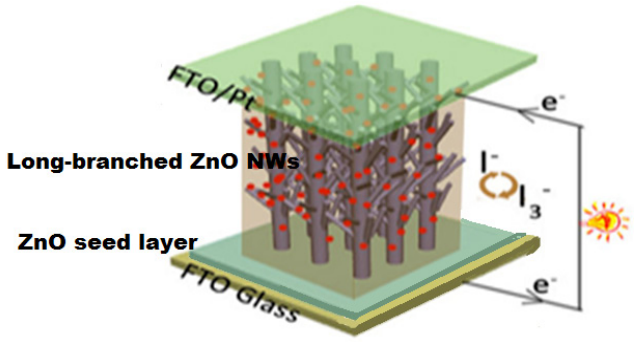

Figure 3: Schematic representation of an assembled Long-Branched ZnO NW DSSC

I-V characterization of the solar cell

To obtain current (I) and voltage (V) data, assembled DSSCs from different photoanodes and sensitized using three different dyes were connected to a Keithely 2400 SMU and illuminated with a solar simulator as shown in Figure 4.

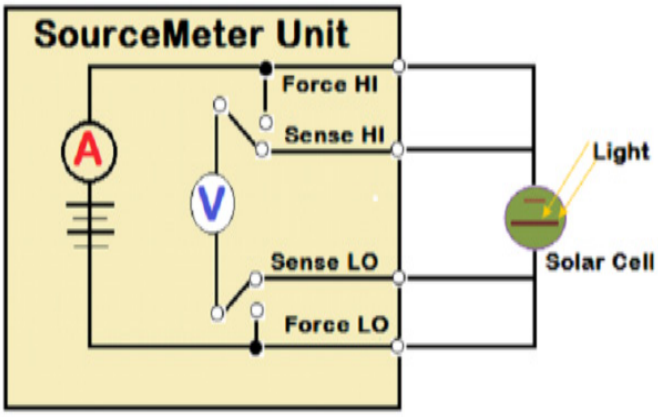

Figure 4: Schematic representation of connection of solar cell to SMU

The DSSC was placed so that the solar irradiance meter indicated a value of $\approx 1000\ W\ m^{-2}$. This illumination caused current to flow to the SMU by acting as an electronic load. An I-V sweep of the DSSC was generated by the SMU and displayed on a computer.

RESULTS AND DISCUSSION

ZnO NPs seeded film

The seeding solution prepared by mixing zinc acetate and sodium hydroxide and incubated at 60° C appeared to decant by itself after 2 h even before centrifugation. The supernatant was discarded and the remaining whitish concentrate was run on a centrifuge. Seeding involved the formation of a thin layer of ZnO film on a FTO-TCO glass substrate to promote nucleation for the growth of NWs by covering the thermodynamic barrier. Equations 1a and 1b shows the reactions which took place (Lee *et al.*, 2011).

$$Zn(CH_3COO)_2 + NaOH \rightarrow Zn(CH_3COO)OH + NaCH_3COO \quad (1a)$$

$$Zn(CH_3COO)OH + NaOH \rightarrow ZnO + NaCH_3COO + H_2O \quad (1b)$$

Heating helps in decomposing of zinc acetate hydroxide $Zn(CH_3COO)OH$ into ZnO NPs. Annealing of the NPs at 210° C was done to enable them to adhere strongly to the substrate. SEM micrographs in Figure 5 show the appearance of the deposited ZnO NPs at different magnifications.

Diameters of three different samples deposited with NPs and SEM images taken at magnification of 50,000 times 50,000 times were measured. Figure 6 shows Gaussian fits to the measured diameters for NPs from each of the three samples and the combined results for all samples.

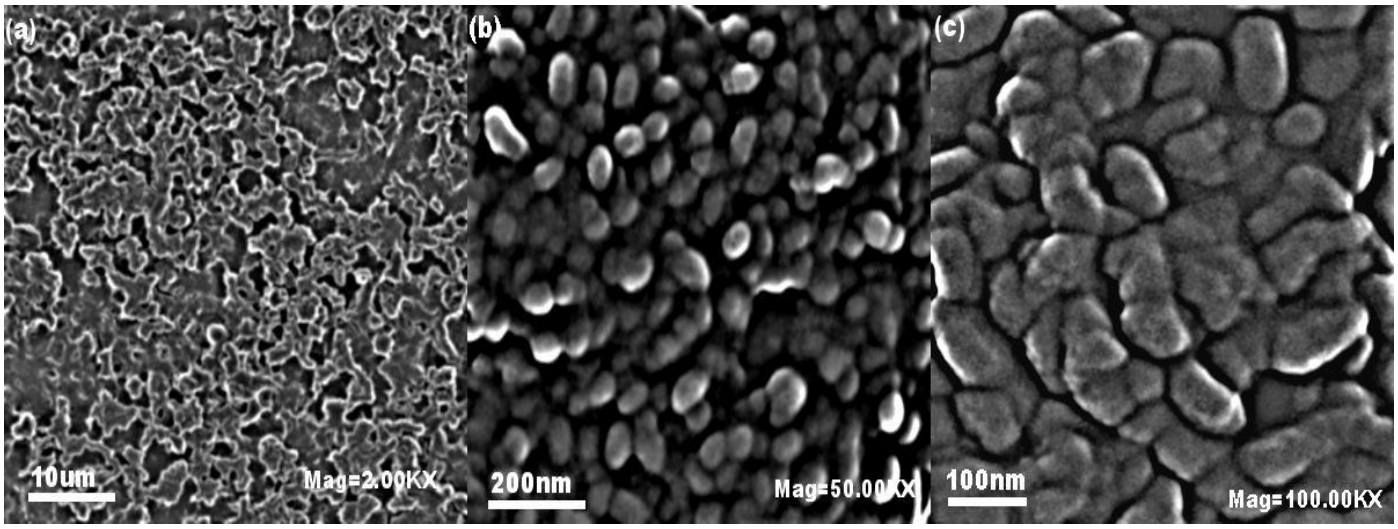

Figure 5: Sem micrograph showing the appearance of ZnO NPs at different magnifications

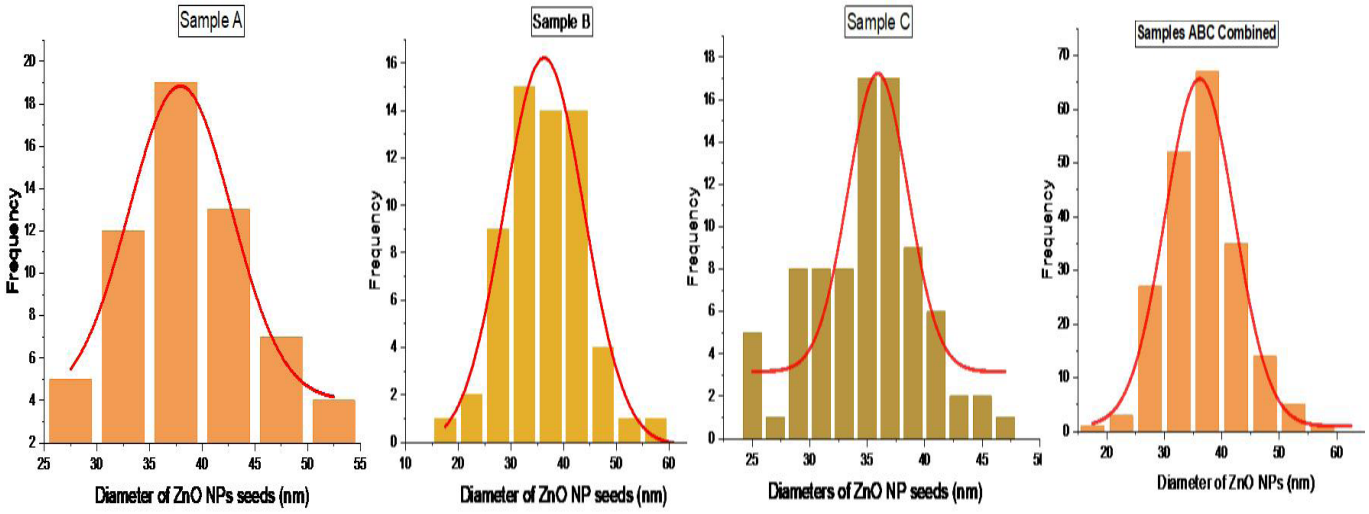

Figure 6: Gaussian fit for NPs samples A, B and C and combined samples

A summary of the analysis of all the NP sizes is recorded in Table 1.

Table 1: Summary of diameters of ZnO NPs taken from three different samples.

ZnO NPs Sample	Range of Diameter (nm)	Mean of the Diameters (nm)	Center xc of the Gauss Fit (nm)	Summary from all the samples (nm)
A	26.4-51.6	38.6	37.9	$\bar{x} = 36.4$
B	17.6-59.8	36.1	36.3	$xc = 36.2$
C	24.3-46.9	35.0	35.9	$\sigma = 6$

From the results, it can be seen that the NP diameters ranged from 24.3 nm to 59.8 nm with a mean diameter $\bar{x} = 36.4\ nm$ compared to $\bar{x} = 34.6\ nm$ reported by Marouf *et al.* (2016). Different sizes of NP are attributed to different rates at which the OH^- anions react with Zn^{2+} cations in the process of forming NPs. The Gaussian fit shows a normal distribution with center value $xc = 36.2 \pm 0.3\ nm$, and standard deviation $\sigma = 6$ nm. The ZnO NP seeds are nearly spherical in shape and produce a granular structure composed of small grains which appear with porosity. The NP film surfaces were slightly non-uniform, which can be attributed to the drop coating method used. However, the glass substrate appears to be densely covered with NP seeds as desired for nucleation and growth of NWs.

ZnO nanowires film

The growth process involves the decomposition of zinc nitrate hexahydrate in the precursor solution according to equation (2) to provide Zn^{2+}

$$Zn(NO_3)_2.6H_2O \rightarrow Zn^{2+} + 2NO_3^- + 6H_2O \quad (2)$$

HMTA also dissociates to form formaldehyde and ammonia as shown in (3a) and (3b) (Sugunan *et al.*, 2006)

$$C_6H_{12}N_4 + 6H_2O \rightarrow 4NH_3 + 6CHCHO \quad (3a)$$

$$NH_3 + H_2O \rightarrow NH_4^+ + OH^- \quad (3b)$$

Zn^{2+} then reacts with OH^- to form $Zn(OH)_2$ which then dissociates to ZnO (Peralta *et al.*, 2011). The whole interaction of HMTA and Zn^{2+} can be summarized by equation (4) as

$$C_6H_{12}N_4 + 8H_2O + 2Zn^{2+} \rightarrow 4NH_4^+ + 6CHCHO + 2ZnO \quad (4)$$

The first role of HTMA, PEI and ammonium hydroxide in the precursor solution is to control the supersaturation of the reactants. High supersaturation levels favor nucleation and lower supersaturation levels favor crystal growth. If a lot of OH^- is produced in a short period, the Zn^{2+} ions in the solution will precipitate out quickly due to the high pH environment and therefore Zn^{2+} would contribute little to the growth of NWs (Sugunan *et al.*, 2006). Therefore, the concentration of OH^- is controlled in the precursor solution to maintain low supersaturation levels during the entire period of NW growth. The precursor solution for Long ZnO growth had a pH = 9.85 at the start (0 h), 8.76 at first replenishing (4 h), 8.66 at second replenishing (8 h) and 8.88 h at the end (12 h). The temperature set at $88°\ C$ fluctuated by $\pm 2°\ C$, conditions which are within the range given in the literature for NW growth (Bu *et al.*, 2008). Zn^{2+} when solvated by water exists in several hydroxyl species whose condensation and hydrolysis at pH between 8 and 9 and temperature above $80°\ C$ results in precipitation of ZnO in 1-D crystals. The second role of HMTA and PEI polymers is structure modification. The polymers attach to nonpolar facets of the NWs and prevent access of Zn^{2+}, leaving only polar faces for epitaxial growth (Law *et al.*, 2004). During annealing, it was observed that the grown side would first turn dark-green before turning back to a crystal white color. This confirmed that the residue polymers of HMTA and PEI had burned away to leave a pure ZnO NW crystal. Figure 7 show the appearance of one NW and the direction of growth as observed by SEM.

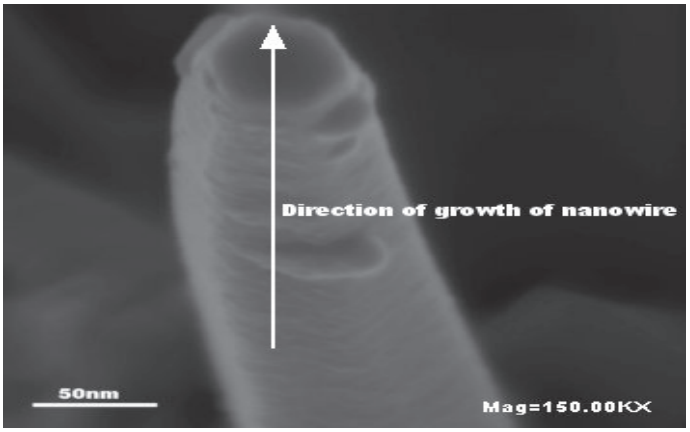

Figure 7: SEM micrograph of a ZnO NW with an arrow showing the direction of growth

More SEM micrographs were taken at different magnifications as shown in Figure 8 to give a clear view of the surface morphology of ZnO NWs. From Figure 8, it was observed that NWs grown were dense for more dye adsorption and most of them were vertically aligned to provide a direct path for the electrons.

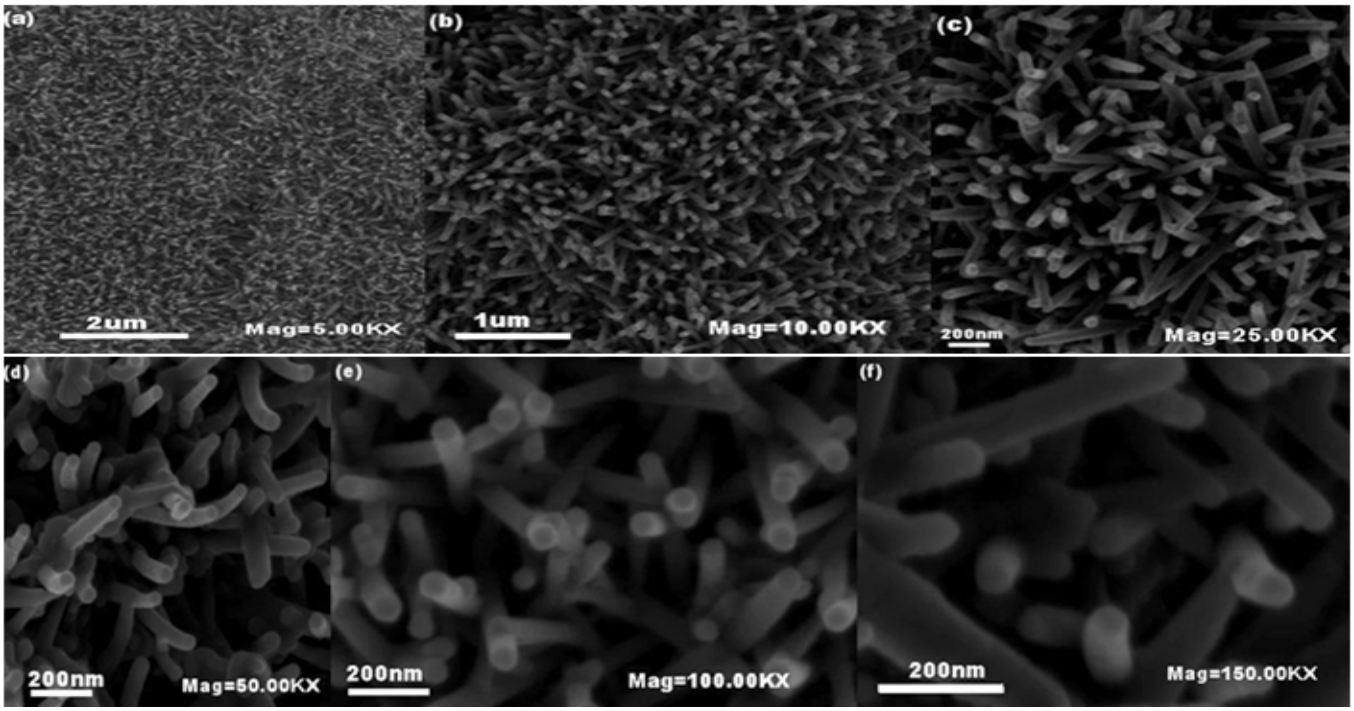

Figure 8: SEM micrograph of ZnO NWs from sample B at magnifications of (a) 5,000 times (b)10,000 times (c) 25,000 times (d) 50,000 times (e) 100,000 times and (f) 150,000 times

Diameters of NWs were measured from three different samples at magnification of 50,000 times. The results for individual and combined samples are summarized in Table 2.

Table 2: Summary of diameters of ZnO NWs from three samples.

ZnO NWs Samples	**Range of Diameter (nm)**	**Mean of the Diameters (nm)**	**Center xc of the Gauss Fit (nm)**	**Summary from all the samples (nm)**
A	48.6-70.8	59.9	61.5	$\bar{x} = 60.6$
B	51.4-69.7	61.0	61.5	$xc = 62.6$
C	42.3-77.8	61.0	61.3	$\sigma = 3$

The diameters of the ZnO NWs were normally distributed. It was noted that NWs had larger diameters than the NP seeds, which is attributed to growth in which Zn^{2+} ions attach themselves to the NP seeds and grow to NWs. The lengths of NWs were measured using SEM images taken from three samples. Figure 9 shows the appearances of the NWs.

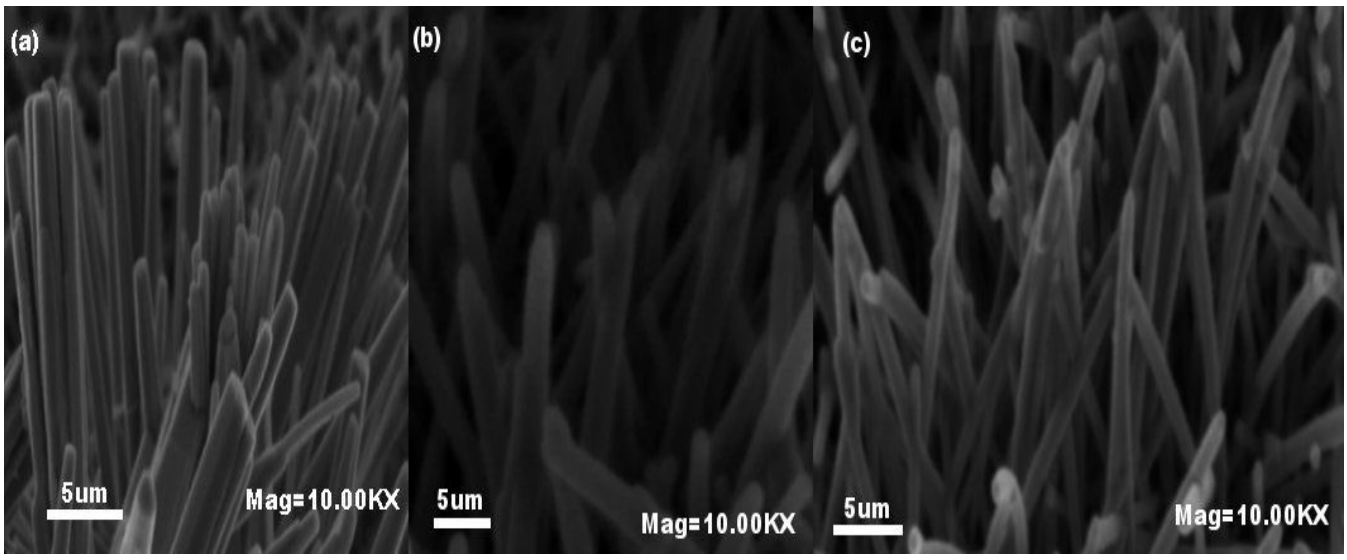

Figure 9: ZnO NWs at magnification of 10,000 times from three samples

The Gaussian fit to lengths from three different samples and combined results are shown in Figure 10.

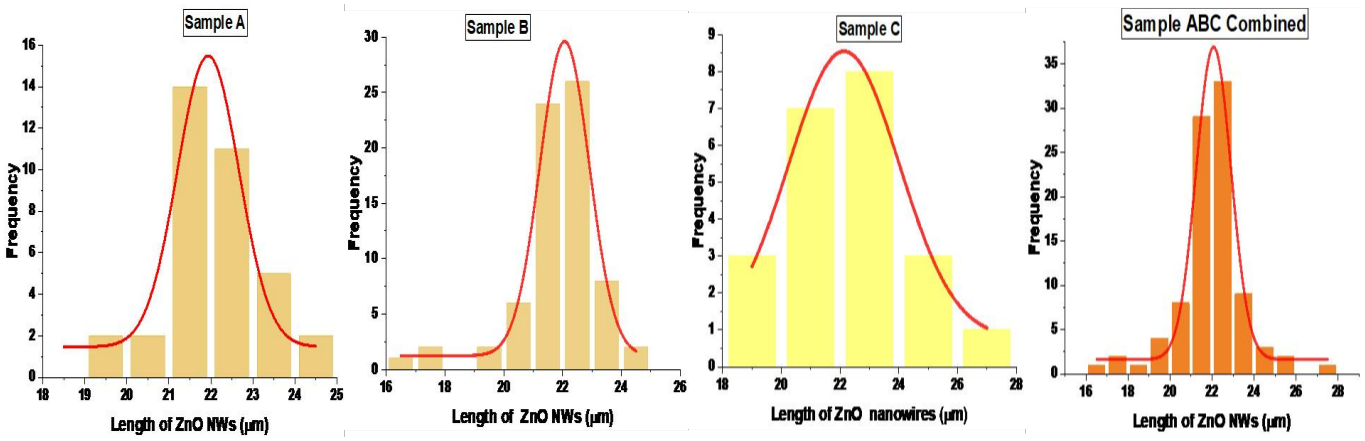

Figure 10: Gaussian fit for the length of NWs for individual samples A, B and C and combined samples

The results of length measurements for three different samples are recorded in the Table 3.

Table 3: Result of length of ZnO NWs from three samples.

ZnO NWs Samples	Range of Length of NWs (µm)	Mean Length of NWs (µm)	Center $xcxc$ of the Gauss Fit (µm)	Summary from all the samples (µm)
A	19.0-24.1	22.1	21.9	$\bar{x} = 22.03$ $xc = 22.07$ $\sigma = 0.8$
B	16.2-23.7	22.2	22.1	
C	18.9-27.4	22.8	22.1	

A summary of all the samples give a mean $\bar{x} = 22.03$ $\bar{x} = 22.03$ mm and a Gaussian fit gave a center value $xc = 22.07\ \mu mxc = 22.07\ \mu m$ with a normal distribution. These results show that longer NWs were grown compared to the ones of length 7-8 µm, 10 µm and 10-15µm grown by Cheng *et al.* (2008), Baxter and Aydil (2005) and Law *et al.* (2005), respectively. The average aspect ratio of the NWs was found by dividing the mean length of the three samples with their mean diameters, and was found to be 364.

Long Branched ZnO nanowires

Branching of the NWs produced shorter 1-D NW branches with a small diameter of origin and growing in various direction from the parent NWs. This was attributed to second seeding, use of a precursor solution with half concentration of the reagent and use of short time of growth. The pH of the precursor was 9.81 at 0 h, 8.88 at replenishing (at 3 h) and 8.90 at the end (6 h). Figure 11 shows SEM micrographs of the ZnO NW branches from sample C at different magnifications.

From Figure 11 the NW branches appear to have grown in different direction from the parent ZnO NWs, hence producing a tree-like appearance. It was also noted that NW branches did not grow on all the parent NWs but only on some favorable ones. This can be attributed to the drop coating method used during the second seeding which could have caused infiltration of NP seeds to only NWs which stood unblocked. Further, it was noted that the branches almost completely covered the original parent NWs because the drop coating method introduced NP seeds to almost every part exposed during second seeding. The measurements taken for the diameters of ZnO NW branches are recorded in Table 4.

The diameters of ZnO NWs branches range between 20.9-62.0 nm with a mean $\bar{x} = 36.9$ nm. Gaussian fits for all the diameters from the three samples gave a center value $xc = 35.9$ nm and were normally distributed.
The length of the NW branches from the parent NWs were also measured from the parent NWs and Gaussian fits done as shown in Figure 12 for every sample and for the combined sample.

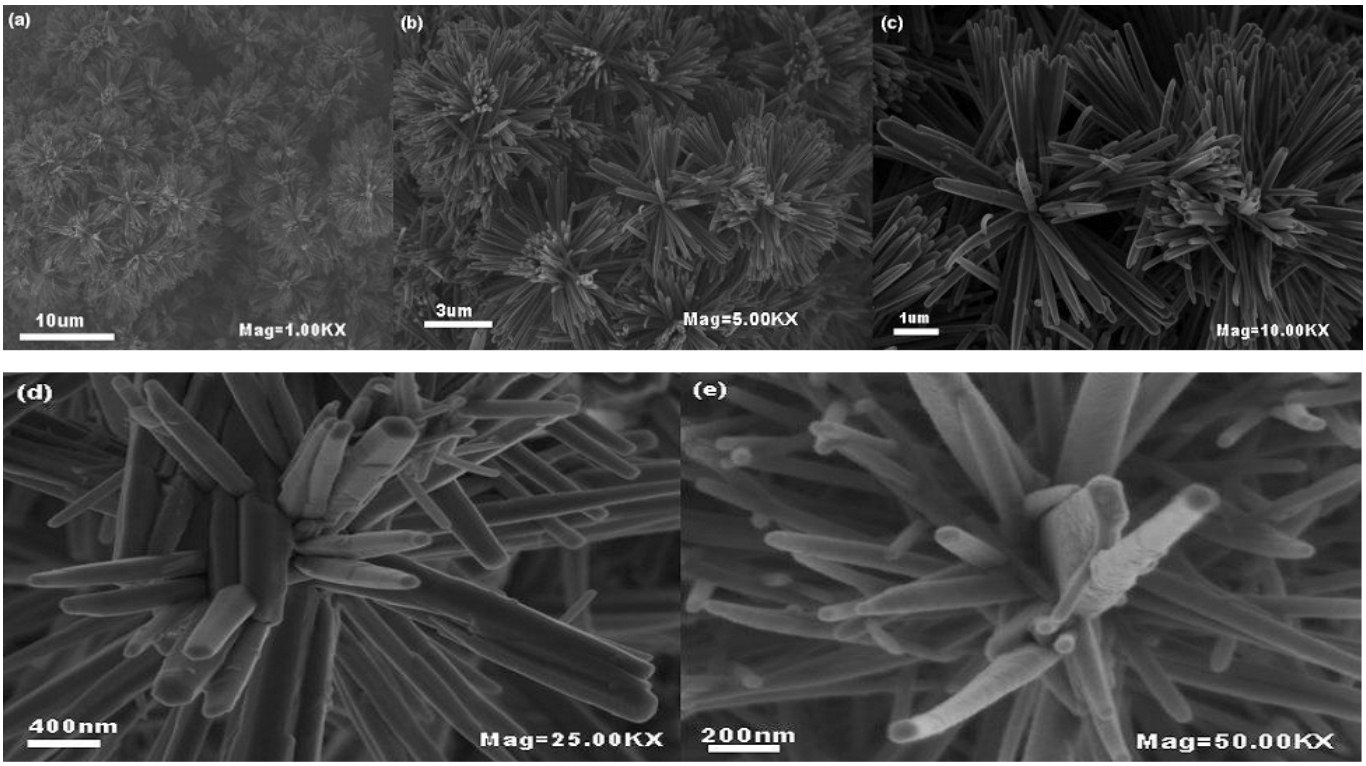

Figure 11: SEM micrographs of ZnO NW branches from sample C at different magnifications (a) 1,000 times (b) 5,000 times (c) 10,000 times (d) 25,000 times and (e) 50,000 times

Table 4: Results of diameter of ZnO NW branches from three samples.

ZnO NW branches Samples	Range of Diameter of Branches (nm)	Mean of the Diameters of Branches (nm)	Center xc of the Gauss Fit (nm)	Summary from all the samples (nm)
A	21.5-50.9	35.2	34.5	$\bar{x} = 36.88$
B	20.9-62.0	36.4	35.4	$xc = 35.90$
C	27.4-57.4	38.3	36.0	$\sigma = 6$

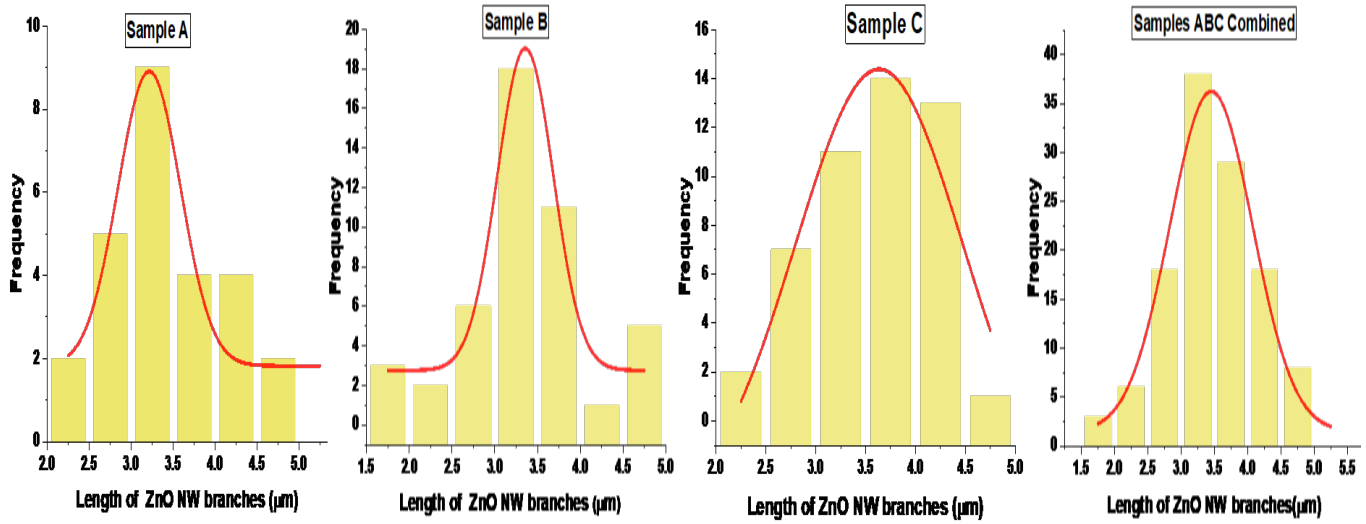

Figure 12: Gaussian fits for ZnO NW branches for samples A, B and C and combined samples

A summary of the results are recorded in Table 5.

Table 5: Result of length of ZnO NWs branches taken from three samples.

ZnO NW Branches Samples	Range of length of ZnO NWs branches (µm)	Mean of length of ZnO NWs branches (µm)	Center xc of the Gauss Fit (µm)	Summary from all the samples (µm)
A	2.3-5.0	3.4	3.2	$\bar{x} = 3.47$
B	1.6-4.9	3.4	3.4	$xc = 3.45$
C	2.0-4.6	3.6	3.6	$\sigma = 0.62$

The range of length of NW branches was 1.6-5.0 µm and were normally distributed with a mean $\bar{x} = 3.47$ µm and $\bar{x} = 3.47$ µm and center value $xc = 3.45$ µm$xc = 3.45$ µm. NW branches had shorter lengths and diameters than the parent NWs.

In general, ZnO films of different nanostructures with clearly distinguished surface morphologies were prepared as shown in Figure 13.

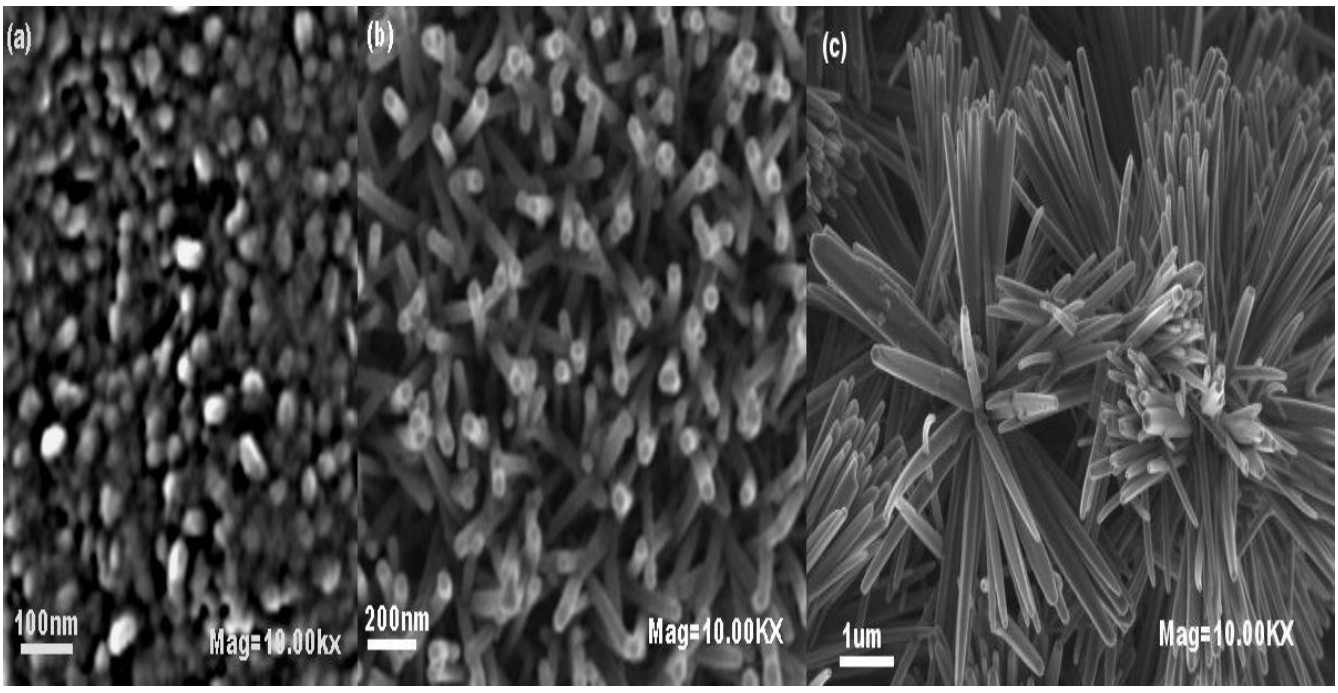

Figure 13: SEM micrograph images for (a) seeded ZnO NP films (b) Long ZnO and (c) Long Branched ZnO NWs

Each of the films have special nanostructure features which are expected to influence dye adsorption, electron collection and transport and overall performance of DSSCs.

Resistivity of the thin films

The sheet resistivity was measured using a four probe method in which a computer is interfaced with a Keithely 2400 SMU using LabVIEW. The results for resistivity were 1.76 $\Omega\,cm^{-1}$ for platinum paste film, 8.69 $\Omega\,cm^{-1}$ for FTO-TCO glass, 14.86 $\Omega\,cm^{-1}$ for ZnO NP films, 36.87 $\Omega\,cm^{-1}$ for Long ZnO NW films, and 47.52 $\Omega\,cm^{-1}$ for long Branched ZnO NW films. The measured resistivity for FTO compared well with the value indicated by the manufacturer, i.e. 8 $\Omega\,cm^{-1}$. It was observed that the sheet resistivity increased from un-deposited FTO-TCO glass substrate to Long Branched ZnO NW films. Sheet resistivity increased as increasing numbers of molecules of ZnO are deposited on FTO-TCO glass substrate.

Optical characterization natural dyes

The absorbance data for the diluted anthocyanin dye, chlorophyll dye and cocktail dye blend obtained were

used to plot spectral graphs. The spectral graphs were analyzed individually to find the dye concentrations and peak positions, then overlaid in one graph in Figure 14 for comparison.

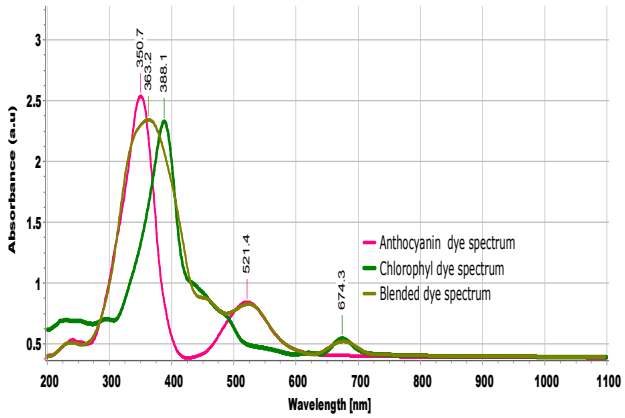

Figure 14: Comparison of the absorbance spectra of anthocyanin, chlorophyll and cocktail dye

From the spectral graph of diluted anthocyanin dye, the concentration was found to be 0.53 M, a value that compared well with the calculated value from dilution, i.e. 0.46 M. This confirms that the dilution process was correctly done. The molar absorption coefficient was calculated for the anthocyanin dye at the highest peak (350.7 nm) with an absorbance of 2.52 absorbance units (a.u.) using the Beer Lambert linear relationship i.e. $A = \varepsilon cl$ where A is the absorption at the highest peak, ε is the molar absorption coefficient, c is the molar concentration, and l is the path length. The molar absorption coefficient is (equation (5)

$$\varepsilon = \frac{A}{cl} = \frac{2.52}{0.53\ M \times 1\ cm} = 4.75\ M^{-1}cm^{-1} \quad (5)$$

Similarly, from the spectrum of the chlorophyll dye, the concentration of the dye was found to be 0.501 M which was the same as the calculated value during quantitation. The molar absorption coefficient at highest peak (388.1 nm) and absorbance of 2.33 a.u. is calculated as $4.65\ M^{-1}cm^{-1}$ using the Beer Lambert linear relationship.

The chlorophyll-anthocyanin dye blend produced a spectrum that showed that the cocktail dye blend had a concentration of 0.51 M which was within the range of anticipated result for blending. The molar absorption coefficient calculated at the highest peak (363.2 nm) was $4.56\ M^{-1}cm^{-1}$. Comparing the three dyes spectral properties, the following observations were made:

(i) Natural dyes have their best absorption features in the UV zone with the maximum peaks at 350.7 nm, 388.2 nm and 363.1 nm for anthocyanin, chlorophyll and the cocktail dye blend, respectively.

(ii) In the VIS zone the cocktail dye blend has the best absorption features since it had two absorption peaks at 523 nm and at 676 nm while anthocyanin and chlorophyll had one peak each at 521.4 nm and at 674.3 nm, respectively.

(iii) The cocktail dye was found to have a wider range of absorption at peak positions as shown by Figure 14. This is confirmed through a calculation of the full width at half maximum (FWHM) in which anthocyanin dye had a FWHM = 70.20 nm, chlorophyll dye had a FWHM = 74.99 nm and the cocktail dye blend had the a FWHM = 117.46 nm, which is the highest of this sample. The FWHM (band width) is a wavelength range used to denote a specific part of the spectrum that passes incident light. A wider absorption band helps in harvesting more light photons because it allows more of the spectrum to pass through (Karki *et al.*, 2012)

(iv) Dye blending in the ratio of 1:1 produces a spectrum which compares well with the original spectra, and thus reduces absorption competition and interference between dyes.

Therefore, the blended dye was found to have the best optical absorbance features which were anticipated to give best performance when used to sensitize the DSSC photo-electrodes.

Optical characterization of thin films

Figure 15 shows the variation of transmittance and absorbance of FTO-TCO glass, ZnO NP films, Long ZnO NW films, Long-Branched ZnO NW films, and Pt paste film with the wavelength. It is observed that all the films had optically transparent windows in UV-VIS-NIR zones starting at 306 nm and proceeding past 1100 nm wavelength. The transparent window enables light to be transmitted through for subsequent absorption by the dye molecules. It is also observed that transmittance increases with increase in wavelength of the incident photon within the visible light region.

FTO-TCO has the highest transmittance, attaining more than 50% at 345 nm and maximum transmittance of 82.76% at 646 nm. Good transmittance of FTO glass substrates is important so as to allow the passage of optimum sunlight to the effective area of the DSSC (Sharma *et al.*, 2018). A general trend of rapid increase in transmittance, attaining a partly constant trend then gradual drop in transmission was observed for all the samples.

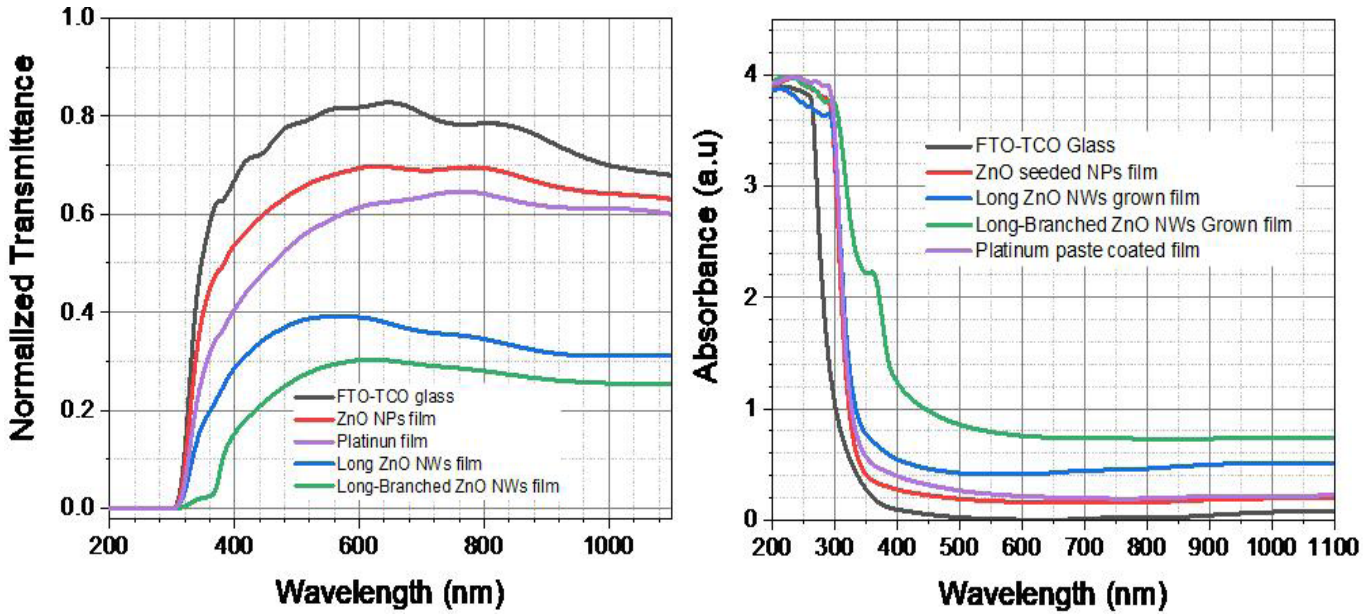

Figure 15: Graphs of normalized transmittance against wavelength and absorbance against wavelength

Absorbance graphs showed an opposite trend to transmittance, this is due negative logarithmic relationship between absorbance (A) and transmittance (T) given by the Beer Lambert relation shown in equation (6) as

$$A = -\log TA = -\log T \quad (6)$$

As the thickness of the film increases, light photons will travel a longer path thus increasing absorption. Thus Long-Branched ZnO NW films attain the highest absorption values indicating the best absorption compared to the other films. Absorption will be improved further by sensitizing the working electrodes with natural dye which has better absorption features in visible light region.

I-V Characterization of illuminated assembled DSSCs

Current (I) and voltage (V) data from the SMU was used to plot I-V curves and determine solar cell parameters for different DSSCs. Figure 16 is an I-V curve for Long Branched ZnO NW DSSCs sensitized with cocktail dye and showing how different solar cell parameters were determined. I_{sc}, I_{max}, V_{oc}, V_{max}, P_{in}, P_{out} and η are short circuit current, maximum current, open circuit voltage, maximum voltage, power input, power output and efficiency, respectively. The efficiency, calculated as $\eta = \frac{V_{oc} I_{sc} FF}{P_{in}}$, is 0.726%

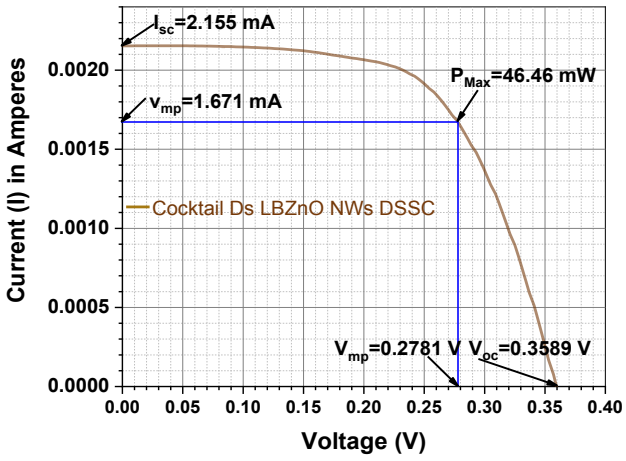

Figure 16: I-V curve for the cocktail dye Long Branched ZnO NW DSSC

Characterization of ZnO NP DSSCs

Figure 17 shows the I-V curves of ZnO NP DSSCs sensitized with different natural dyes. It was observed that blended dye gives better solar cell parameters ($V_{oc} = 0.343$ V and $I_{sc} = 1.66$ mA) than pure anthocyanin ($V_{oc} = 0.330$ V and $I_{sc} = 1.507$ mA) and pure chlorophyll ($V_{oc} = 0.320$ V and $I_{sc} = 1.28$ mA) dyes.

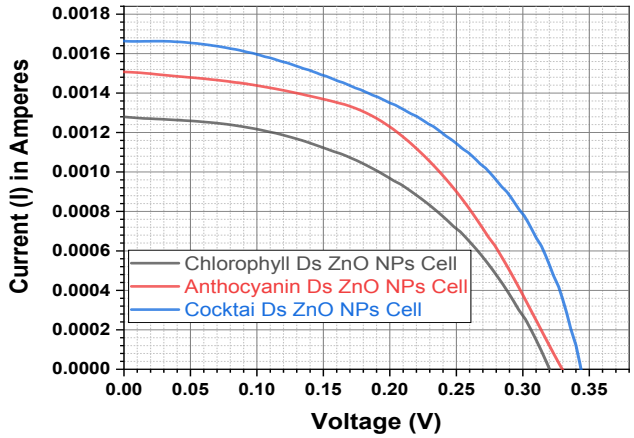

Figure 17: I-V Curves of ZnO NPs DSSCs

The overall output characteristic of ZnO NP cells sensitized with cocktail dye ($\eta = 0.448\ \%$) is better than that of pure anthocyanin dye ($\eta = 0.379\ \%$) and chlorophyll dye ($\eta = 0.303\ \%$) respectively. This is attributed to better absorption properties (3 maximum absorption peaks and wide absorption range at peak position) which allowed more light to be absorbed for excitation of dye molecules. However, the overall performance of DSSC from ZnO NP films appears low compared to Krobthong *et al.* (2020) whose cells were sensitized with inorganic N719 dye and had an efficiency of 2.51%. The low performance can be attributed to low dye adsorption to the NP films due to their compactness and small size of NP crystals which leads to small surface area for dye adsorption. Small sized NPs also lead to short electron pathways hence increasing electron-hole recombination losses.

I-V Characterization of Long ZnO NW DSSCs

I-V characterization for Long ZnO DSSCs sensitized with the cocktail dye blend had the best solar cell parameters with $V_{oc} = 0.339\ V$ and $I_{sc} = 1.98\ mA$. Sensitizing with anthocyanin and chlorophyll gave $V_{oc} = 0.339\ V$ and $I_{sc} = 1.58\ mA$ and $V_{oc} = 0.336\ V$ and $I_{sc} = 1.76\ mA$ respectively. All I-V curves are plotted in Figure 18 and solar cell parameters summarized in Table 6. Long ZnO NW cells sensitized with cocktail dye, anthocyanin dye and chlorophyll dye had efficiencies of 0.570%, 0.420% and 0.400% respectively. This is a better performance compared to NP DSSCs which can be attributed to improved electron transport, quantum confinement, reduced recombination losses due to long electron paths and better dye loading due to the large surface area associated with long NWs.

I-V Characterization of Long Branched ZnO NWs DSSCs

I-V characterization for Long Branched ZnO NW DSSCs sensitized with cocktail dye blend had the best solar cell parameters wit h $V_{oc} = 0.359\ V$ and $I_{sc} = 2.16\ mA$. Sensitizing with anthocyanin and chlorophyll gave $V_{oc} = 0.345\ V$ and $I_{sc} = 2.07\ mA$ and $V_{oc} = 0.354\ V$ and $I_{sc} = 1.87\ mA$ respectively. The cells appear to perform better than those from Long ZnO NW cells with efficiencies of 0.726%, 0.626% and 0.536% for Long Branched ZnO NWs DSSC sensitized with cocktail dye, anthocyanin dye and chlorophyll dye respectively. This can be attributed to improved electron collection and transport, adsorption of more dyes molecules on NW branches and reduced recombination losses due to long electron paths taken by electrons through the branches and parent NWs. In all nanostructured DSSCs, it is also observed that those sensitized with cocktail dye blend performed better than those sensitized with pure dyes.

Comparison of I-V characterization of all assembled DSSCs

Figure 18 show I-V curves for all assembled DSSCs on the same axis and Table 6 gives a summary of the performance of the three categories of DSSC. In all categories of DSSCs, we observe that blended dye produced a better performance compared to pure dyes. This is attributed to improved light absorption features observed during optical analysis of pure and blended dyes. The blended dye has a wider range of absorption at peak positions and also has many more absorption peaks in the UV-Vis regions. Anthocyanin dye sensitizer is noted to perform better than chlorophyll dye when used as a pure sensitizer. This is attributed to its higher value of absorbance at highest peak (2.52 a.u) compared to that of chlorophyll dye (2.33 a.u). We can therefore conclude that the highest absorption peak of a pure dye is more significant in determining DSSC performance than the absorption range determined by FWHM.

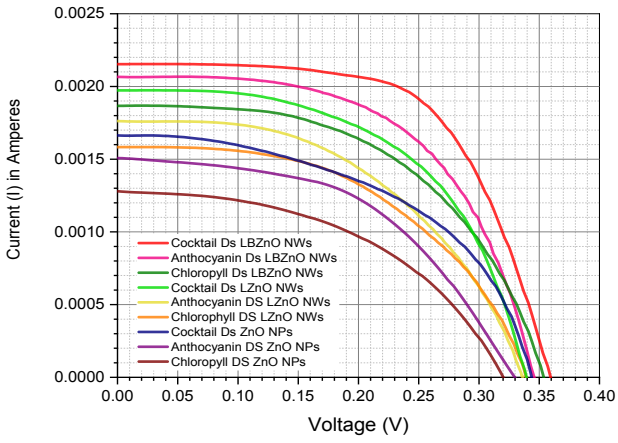

Figure 18: I-V Curve for all assembled DSSCs

It is also observed that in all sensitization, chlorophyll ZnO NW DSSCs performed better than Long ZnO DSSCs while Long ZnO DSSCs performed better than ZnO NP DSSCs. This shows that there is an improvement in performance of DSSCs as we move from NP nanostructure of the photoanode to NW nanostructure. Further, branching of NWs improves the performance of DSSCs because of increased dye adsorption and dye loading.

Generally, in changing nanostructure from NPs to chlorophyll NWs we improve the performance of DSSCs. Growth and branching of NWs increases charge collection and transport, decreases electron hole recombination and increases dye loading in DSSCs. Also, natural dyes when blended in the ratio 1:1 produce large light harvesting capacities in UV-VIS region, thereby improving the performance of DSSCs.

Table 6: A comparison of the performance of DSSCs.

Film of working Electrode	Sensitizing Dye	V_{oc} (V)	I_{sc} (A)	V_{mp} (V)	I_{mp} (A)	Fill Factor (F.F)	Effective Cell Area (cm^2)	P_{in} (W)	%Efficiency, η
Long Branched ZnO NWs	Cocktail	0.359	0.00216	0.278	0.00167	0.601	0.64	0.064	0.726
	Anthocyanin	0.345	0.00207	0.259	0.00155	0.561	0.64	0.064	0.626
	Chlorophyll	0.353	0.00187	0.255	0.00135	0.519	0.64	0.064	0.536
Long ZnO NWs	Cocktail	0.339	0.00198	0.250	0.00146	0.544	0.64	0.064	0.570
	Anthocyanin	0.339	0.00158	0.238	0.00113	0.503	0.64	0.064	0.420
	Chlorophyll	0.336	0.00176	0.234	0.00123	0.487	0.72	0.072	0.400
ZnO NPs	Cocktail	0.343	0.00166	0.243	0.00118	0.502	0.64	0.064	0.448
	Anthocyanin	0.330	0.00151	0.230	0.00105	0.488	0.64	0.064	0.378
	Chlorophyll	0.320	0.00128	0.218	0.00087	0.466	0.63	0.063	0.303

CONCLUSION

Based on results obtained in this work, performance and characteristic of fabricated ZnO DSSCs depends on the type of nanostructure and dye used for sensitization. ZnO has the potential of producing high performing DSSCs by utilizing its physical and chemical properties which enables it to be synthesized to various nanostructures. ZnO NPs with mean diameter of 36.4 nm which where nearly spherical were deposited, forming a granular surface which was slightly non-uniform as observed from SEM images. The dye loading into tortuous and low thickness NP films was low and therefore light harvesting capacity was also low. Electron transport in NP films is limited by trapping/de-trapping processes which significantly reduce the electron diffusion length. The efficiencies of DSSCs assembled from NP films were 0.448%, 0.379% and 0.303% for DSSCs sensitized with cocktail dye, anthocyanin dye and chlorophyll dye respectively. Long ZnO NWs with a mean diameter of 60.6 nm and length of 22.03 μm were grown. SEM Images showed that they were generally vertically aligned and therefore provided a direct path for electron transport after collection from the excited dye molecules. The DSSCs assembled from Long ZnO NWs had efficiencies of 0.570%, 0.420% and 0.400% when sensitized with cocktail dye, anthocyanin dye and chlorophyll dye respectively. Branching of Long ZnO further improves charge collection and provides several paths for electrons transport to conductive glass. SEM images showed that several NW branches were grown with mean diameter of 36.9 μmμm and mean length of 3.5 μmμm. The branches were facing all directions from the parent NWs. Branching is believed to have improved dye adsorption and dye loading hence increasing light harvesting efficiency and consequently the performance of the DSSC. The efficiencies of Long Branched ZnO NW assembled DSSCs were 0.726%, 0.626% and 0.536%

when sensitized with cocktail dye, anthocyanin dye and chlorophyll dye respectively.

We also conclude that less costly organic dyes sensitizers could be cheaper alternatives to the more expensive metal complex dyes. The organic dyes used here were found to have good absorption features from 230-770 nm within the UV-VIS region of electromagnetic radiation where most of the solar energy received on the Earth's surface lies. When two pure organic dyes of anthocyanin and chlorophyll are blended in ratio of 1:1, they give better absorption features than pure dyes and consequently recorded better performance when used to sensitize ZnO films of different nanostructures: ZnO NPs, Long ZnO and long Branched ZnO NWs for DSSC. Anthocyanin dye extract from mulberries was found to have more potential for application as a sensitizer because it produced better performing DSSC than those sensitized with chlorophyll dye from spinach. This was attributed to its high peak absorbance rate within a short wavelength.

ACKNOWLEDGEMENT

This work was supported by the Africa Development Bank (AfDB). Authors would like to acknowledge Kenyatta University Physics Department, Physical and Biological Sciences laboratories at Chuka University and University of Nairobi, and the University of Pretoria, South Africa for providing access to their facilities

REFERENCES

Adedokun, O., Titilope, K., and Awodugba, A. O. (2016). Review on natural dye-sensitized solar cells (DSSCs). *International Journal of Engineering Technologies IJET*, *2*(2), 34–41.

Baxter, J. B., and Aydil, E. S. (2005). Nanowire-based dye-sensitized solar cells. *Applied Physics Letters*, *86*(5), 053114.

Berni, A., Mennig, M. and Schmidt, H. (2004). *Doctor blade*. In *Sol-gel technologies for glass producers and users*. Springer, Boston, MA. Pp. 89–92.

Bu, S., Cui, C., Wang, Q., and Bai, L. (2008). Growth of ZnO nanowires in aqueous solution by a dissolution-growth mechanism. *Journal of Nanomaterials*, *43*, 1–5, 610541.

Chen, W., Zhang, H., Hsing, I. M., and Yang, S. (2009). A new photoanode architecture of dye sensitized solar cell based on ZnO nanotetrapods with no need for calcination. *Electrochemistry Communications*, *11*(5), 1057–1060.

Chen, Z., Li, F., and Huang, C. (2007). Organic D-π-A dyes for dye-sensitized solar cell. *Current Organic Chemistry*, *11*(14), 1241–1258.

Cheng, C., and Fan, H. J. (2012). Branched nanowires: synthesis and energy applications. *Nano Today*, *7*(4), 327–343.

Cheng, H. M., Chiu, W. H., Lee, C. H., Tsai, S. Y., and Hsieh, W. F. (2008). Formation of branched ZnO nanowires from solvothermal method and dye-sensitized solar cells applications. *The Journal of Physical Chemistry*, *112*(42), 16359–16364.

Chopra, K. L., Paulson, P. D., and Dutta, V. (2004). Thin-film solar cells: an overview. *Progress in Photovoltaics: Research and Applications*, *12*(2-3), 69–92.

Chu, Y., and Meisen, P. (2011). Review and comparison of different solar energy technologies. *Global Energy Network Institute (GENI), San Diego, CA.*, *2011*(1), 1–52.

Green, M. A. (1982). *Solar cells: operating principles, technology, and system applications*. Englewood Cliffs, NJ, Prentice-Hall, Inc., 288.

Green, M. A. (2003). Crystalline and thin-film silicon solar cells: state of the art and future potential. *Solar Energy*, *74*(3), 181–192.

Hara, K. and Mori, S., (2011). *Dye-sensitized solar cells. Handbook of photovoltaic science and engineering*. Pp. 642–674.

Hess, G. (2005). Basic research needs for solar energy utilization, US Department of Energy. *Chemical Engineering News*, *83*, 12.

Kabir, F., Bhuiyan, M. M. H., Manir, M. S., Rahaman, M. S., Khan, M. A., and Ikegami, T. (2019). Development of dye-sensitized solar cell based on combination of natural dyes extracted from Malabar spinach and red spinach. *Results in Physics*, *14*, 102474.

Et alw, I. B., Nakarmi, J. J., Mandal, P. K., and Chatterjee, S. (2012). Absorption spectra of natural dyes and their effect on efficiency of ZnO based dye-sensitized solar cells. *Nepal Journal of Science and Technology*, *13*(1), 179–185.

Krobthong, S., Nilphai, S., Choopun, S., and Wongrerkdee, S. (2020). Synthesis and characterization of ZnO nanoparticle films its application in dye-sensitized solar cells. *Digest Journal of Nanomaterials and Biostructures*, *15*(3), 885–894.

Law, M., Greene, L. E., Johnson, J. C., Saykally, R., and Yang, P. (2005). Nanowire dye-sensitized solar cells. *Nature Materials*, *4*(6), 455–459.

Law, M., Goldberger, J., and Yang, P. (2004). Semiconductor nanowires and nanotubes. *Annual Review Material Research*, *34*, 83–122.

Lee, G. J., Min, S. K., Oh, C. H., Lee, Y., Lim, H., Cheong, H., ... Han, S. H. (2011). Effects of seed layers on structural, morphological, and optical properties of ZnO nanorods. *Journal of Nanoscience and Nanotechnology*, *11*(1), 511–517.

Marouf, S., Beniaiche, A., Guessas, H., and Azizi,

A. (2016). Morphological, structural and optical properties of ZnO thin films deposited by dip coating method. *Materials Research*, *20***,** 88–95.

Martín, C., Ziółek, M., and Douhal, A. (2016). Ultrafast and fast charge separation processes in real dye-sensitized solar cells. *Journal of Photochemistry and Photobiology C: Photochemistry Reviews*, *26*, 1–30.

Martineau, D. (2012). *Dye Solar Cells for Real. The Assembly Guide for Making Your Own Solar Cells.* Switzerland: Solaronix SA., *2012*(1), 1–40.

Md Yunus, N. A., Nik Aman, N. H., and Khoshsirat, N. (2015). Comparison between thin-film solar cells and copper–indium–gallium–diselenide in Southeast Asia. *IET Renewable Power Generation*, *9*(8), 1079–1086.

Onyia, A. I., Ikeri, H. I., and Chima, A. I. (2020). Surface and quantum effects in nanosized semiconductor. *American Journal of Nano Research and Applications*, *8*(3), 35–41.

O'Regan, B., and Grätzel, M. (1991). A low-cost, high-efficiency solar cell based on dye-sensitized colloidal TiO_2 films. *Nature*, *353*(6346), 737–740.

Ossai, A. N., Alabi, A.B., Ezike, S.C., and Aina. A. O. (2020). Zinc oxide-based dye-sensitized solar cells using natural and synthetic sensitizers. *Current Research in Green and Sustainable Chemistry*, *3*(2020), 100043.

Peralta, M. D. L. R., Serrano, J. G., and Pal, U. (2011). Morphology defined ZnO nanostructures through microwave assisted chemical synthesis: growth mechanism, defect structure, and emission behaviours. *Advanced Science Letters*, *4*, 1–8.

Sharma, K., Sharma, V., and Sharma, S. S. (2018). Dye-sensitized solar cells: fundamentals and current status. *Nanoscale Research Letters, 13*(1), 381.

Sugunan, A., Warad, H. C., Boman, M., and Dutta, J. (2006). Zinc oxide nanowires in chemical bath on seeded substrates: role of hexamine. *Journal of Sol-Gel Science and Technology*, *39*(1), 49–56.

Xia, Y., Yang, P., Sun, Y., Wu, Y., Mayers, B., Gates, B., ... Yan, H. (2003). One-dimensional nanostructures: synthesis, characterization, and applications. *Advanced Materials*, *15*(5), 353–389.

Xu, C., Shin, P., Cao, L., and Gao, D. (2009). Preferential growth of long ZnO nanowire array and its application in dye-sensitized solar cells. *The Journal of Physical Chemistry C*, *114*(1), 125–129.

Xu, F., and Sun, L. (2011). Solution-derived ZnO nanostructures for photoanodes of dye-sensitized solar cells. *Energy and Environmental Science*, *4*(3), 818–841.

Yeo, J., and Ko, S. H. (2014). *Hierarchical nanostructures for solar cells*. Hierarchical Nanostructures for Energy Devices, *35*, 59.

Zhang, G., Bala, H., Cheng, Y., Shi, D., Lv, X., Yu, Q., and Wang, P. (2009). High efficiency and stable dye-sensitized solar cells with an organic chromophore featuring a binary π-conjugated spacer. *Chemical Communications*, *16*, 2198–2200.

Zhang, Q. and Cao, G. (2011). Nanostructured photoelectrodes for dye-sensitized solar cells. *Nano Today*, *6*(1), 91–109.Ě